

# Photocatalytic effect of nano-TiO<sub>2</sub> loaded cement on dye decolorization and *Escherichia coli* inactivation under UV irradiation

Nasim Ganji<sup>1</sup> · Ali Allahverdi<sup>1</sup> · Fereshteh Naeimpoor<sup>2</sup> · Mostafa Mahinroosta<sup>1</sup>

Received: 27 August 2015 / Accepted: 19 November 2015 / Published online: 27 November 2015  
© Springer Science+Business Media Dordrecht 2015

**Abstract** In the present study, titanium dioxide (TiO<sub>2</sub>) nano-particles were synthesized by sol–gel technique and then used to provide nano-TiO<sub>2</sub> loaded cement samples at 1, 5, and 10 wt% for investigation of Malachite green pigment decomposition and *Escherichia coli* inactivation under UV irradiation. Surveys conducted on the synthesized TiO<sub>2</sub> nano-particles showed a 100 % anatase phase with a mean particle size of 66.5 nm, surface area of 64.352 m<sup>2</sup> g<sup>-1</sup>, and a porosity volume of 0.1278 cm<sup>3</sup> g<sup>-1</sup>. Cement samples containing this catalyst exhibited stronger photocatalytic properties as compared to the same amount of pure catalyst. Considering both photocatalytic performance and cost of catalyst, 5 wt% titanium dioxide was suggested to be added to cement. By addition of 1 wt% polycarboxylic copolymer as super-plasticizer to the cement paste, the photocatalytic sample activities were reinforced so that a similar performance could be obtained at 1 wt% catalyst as compared to 5 wt% catalyst without super-plasticizer.

**Keywords** Decolorization · Nanoparticles · Photocatalysts · Sol–gel chemistry · Titanium dioxide

---

✉ Ali Allahverdi  
ali.allahverdi@iust.ac.ir

Nasim Ganji  
nassim.ganji@gmail.com

Fereshteh Naeimpoor  
fnaeim@iust.ac.ir

Mostafa Mahinroosta  
mahinroosta2010@gmail.com

<sup>1</sup> Cement Research Center, School of Chemical Engineering, Iran University of Science and Technology, Narmak, Tehran 1684613114, Iran

<sup>2</sup> Biotechnology Laboratory, School of Chemical Engineering, Iran University of Science and Technology, Narmak, Tehran 1684613114, Iran

## Introduction

Over the past decade several experimental and industrial attempts have been made to improve self-cleaning properties of building cements with interior or exterior application by addition of wax and heavy paraffin at diverse compositions. This approach is indeed an imitation of the protective effect found in *Nelumbo nucifera* (Lotus effect) within which a structured hydrophobic film protects the leaves from environmental pollutants. However, this hydrophobic coating will be soon deteriorated when exposed to air or UV light [1]. Conversely, photocatalytic degradation of harmful pollutants by irradiated particles in the environment has received considerable attention [2]. Applications include the photocatalytic, anti-bacterial, self-cleaning, self-sterilizing materials, air purification coatings and pavements. Titanium dioxide is the most widely used photocatalyst in the field of construction materials. The extensive use of  $\text{TiO}_2$  is attributed to its characteristics of being relatively inexpensive, safe, non-toxic, chemically stable, highly photocatalytic compared to other metal oxide photocatalysts, effective under weak solar irradiation in atmospheric environment and compatible with traditional construction materials, such as cement, without changing any original performance [3].

The first application of  $\text{TiO}_2$  goes back to 1910 when it was used as a pigment instead of toxic lead oxides which were most often used as a pigment for primer paints for iron objects. Much later in 1972, it was found that water can be decomposed into  $\text{H}_2$  and  $\text{O}_2$  by  $\text{TiO}_2$ . It was after this observation that many photoactive properties of  $\text{TiO}_2$  were discovered and these in turn extended the application fields of  $\text{TiO}_2$  [4]. In 1985,  $\text{TiO}_2$  was used as microbicide in photo-killing *Lactobacillus acidophilus* and *Escherichia coli* (*E. coli*) [5]. This antibacterial property was then used to manufacture ceramic tiles coated with photoactive  $\text{TiO}_2$  in 1995 with application in the floors and walls in several hospital operating rooms, where sterile conditions are crucial. In 1997, Wang et al. [6] produced highly hydrophilic  $\text{TiO}_2$  surfaces with anti-fogging and self-cleaning properties. Recently, self-sterilizing  $\text{TiO}_2$  based building materials have been produced and used widely. Many researchers combine  $\text{TiO}_2$  with construction materials taking advantage of various methods to produce novel building materials with photoactive functions such as air cleaning [7–9], self-cleaning [10–12], decolorization [13–15], sterilization, anti-bacterial and anti-algae [16–21]. Investigations on the antibacterial property of  $\text{TiO}_2$  have so far been majorly conducted on glasses and ceramics containing  $\text{TiO}_2$ . However, few studies have been conducted on cement containing  $\text{TiO}_2$  with antibacterial and self-sterilization properties.

This work is an attempt to produce self-cleaning and antibacterial nano- $\text{TiO}_2$  loaded cement that can be applied as a coating on the intended surfaces. One other advantage of photocatalytic cements is that they are economical alternatives at large scale manufacturing compared to the other materials having the same function.  $\text{TiO}_2$  nano-particles were prepared by the sol–gel method. X-ray diffraction (XRD) was used for phase analysis and transmission electron microscopy (TEM) and field emission scanning electron microscopy (FE-SEM) techniques were used for microstructure studies. UV–Vis absorption and BET methods were also performed

for further investigations. In the next step, this material has been used for making cement disks and finally, the ability of these disks in deactivation of bacteria and degradation of organic dye has been studied. The organic dye in the present study is Malachite green. The reasons for choosing Malachite green as the organic model are: (1) it is environmentally stable and severely toxic to a wide range of animals. It causes serious public health hazards and also poses potential environmental problem. Both clinical and experimental observations reported so far reveal that Malachite green is a multi-organ toxin. It decreases food intake, growth and fertility rates; causes damage to the liver, spleen, kidney and heart; inflicts lesions on the skin, eyes, lungs and bones; and produces teratogenic effects. Malachite green is highly cytotoxic to mammalian cells. Incidences of tumor in the lungs, breast and ovary have also been reported from rats exposed to Malachite green. It also acts as a respiratory enzyme poison [22], (2) Malachite green has properties that make it difficult to remove from aqueous solutions and also toxic to major microorganisms. Though, the use of this dye has been banned in several countries and not approved by US Food and Drug Administration, it is still being used in many parts of the world due to its low cost, easy availability and efficacy and to lack of a proper alternative [23]. Also, it has been reported that no significant degradation of Malachite green is observed due to direct exposure to UV irradiation [24, 25].

## Experimental details

### Materials

The following commercial reagents (Merk, Germany) were used: tetraisopropyl orthotitanate Ti(OC<sub>3</sub>H<sub>7</sub>)<sub>4</sub>; absolute grade ethanol (EtOH), methanol (MeOH) and ethanolamine (EA) all at 99 % purity and Malachite green oxalate dye (C<sub>23</sub>H<sub>25</sub>·CIN<sub>2</sub>) at 96 % purity. Pure TiO<sub>2</sub> samples were prepared by the sol–gel technique.

**Table 1** Physical and chemical properties of Portland cement

Physical properties					
Density (g cm <sup>-3</sup> )					3.13
Blaine specific surface area (cm <sup>2</sup> g <sup>-1</sup> )					2954
Chemical properties					
Chemical composition (wt%)				Bogue's potential phase composition (wt%)	
CaO	63.90	SO <sub>3</sub>	2.07	C <sub>3</sub> S	56.53
SiO <sub>2</sub>	20.83	K <sub>2</sub> O	0.59	C <sub>2</sub> S	17.16
Al <sub>2</sub> O <sub>3</sub>	4.56	Na <sub>2</sub> O	0.15	C <sub>3</sub> A	5.84
Fe <sub>2</sub> O <sub>3</sub>	3.69	Free-lime	0.85	C <sub>4</sub> AF	11.23
MgO	2.56	LOI*	1.51		

\* Loss on ignition

*E. coli* (PTCC 1395) was obtained from the Persian Type Culture Collection and Luria–Bertani (LB) culture medium from Sigma-Aldrich was used for its cultivation. Type II Portland cement (PC) in accordance with ASTM standard was used to prepare cement disks with a diameter of 1 cm. Physical and chemical properties of PC are shown in Table 1. Polycarboxylic copolymer (Merk, Germany) was used as super-plasticizer.

### Preparation of catalyst

A mixture of 5 g tetraisopropyl orthotitanate with 5.36 g EA was prepared and stirred for 2 h. To this mixture, a further 5.36 g EA in 0.32 g water was slowly added in droplets and the solution was stirred until the sol was formed. The sol was then kept at room temperature for 24 h until gel formation. The prepared gel was first dried at 150 °C for 3 h and then calcined at 500 °C for 4 h to obtain crystallized structures of TiO<sub>2</sub>.

### Characterization of catalyst

To analyze the prepared catalyst, samples were dissolved in distilled water and their spectral properties were determined using UV–Vis absorbance spectrum on a GBC Cintra 40 UV–Visible spectrophotometer. To determine the identity of any phase present in the samples and their crystalline size, XRD pattern was obtained by using CuK $\alpha$  radiation at 295 K. A 100 % anatase phase was recognized and its average crystallite size then determined according to the Scherrer equation using FWHM data after correction of the instrument peak broadening. The specific area was determined by BET isotherm using N<sub>2</sub> at 77 K. The morphology of particles was investigated using field emission scanning electron microscopy (Sigma, Zeiss) with EDS and Map detector (Oxford Instruments, England) at a voltage of 15 kV and transmission electron microscopy (TEM) image of the synthesized TiO<sub>2</sub> nanoparticles was prepared on a Philips (Amsterdam, The Netherlands) transmission electron microscope operated at an accelerating voltage of 100 kV.

### Preparation of cement disks

A mechanical mixing was used for the purpose of loading synthesized TiO<sub>2</sub> nanoparticles on PC, so that they were added to the PC powder at 1, 5 and 10 wt% and the mixture was homogenized by the APV homogenizer (BT12.51) for 2 min. Water was further added to reach a mixture containing 28 wt% water, prior to the formation of disks and then the resulting paste was manually homogenized. Cement disks at 1 cm diameter were then kept in a chamber at relative humidity of more than 95 % for 24 h.

To reduce the pH of disks and make them ready for antibacterial test, they were exposed to water flow and their pH was measured periodically until reaching pH = 7.

To investigate the effect of super-plasticizer on the photocatalytic property of samples, 1 wt% polycarboxylic copolymer super-plasticizer was added to three samples as given in Table 2.

The water required to maintain a constant workability in super-plasticized paste was measured to be 25 wt% of the cement based on the flow table test in accordance with ASTM C230. The ability of these disks in deactivation of bacteria and degradation of organic dye was compared with control samples without super-plasticizer.

### Cultivation of *E. coli*

Cultivation of bacterial cells was performed according to Caballero et al. [26]. *E. coli* was sub-cultured on Petri dishes containing LB medium supplemented with agar at 37 °C for 24 h. A loopful of fresh culture was inoculated into 50 ml of LB medium containing in g l<sup>-1</sup>: NaCl, 5; peptone, 10; and yeast extract, 5. Culture was then incubated aerobically at 159 rpm in a shaker at 37 °C until the mid exponential phase of bacterial growth [equivalent to an optical density (OD) of 0.8 at 600 nm]. Subsequently, this culture was centrifuged at 4000 rpm and 4 °C for 10 min. The collected bacterial cells were then washed three times to remove medium components and cells were re-suspended in sterile saline solution containing 0.9 % NaCl to obtain a cell density of 10<sup>8</sup> CFU (colony forming unit) per milliliter. This cell suspension was stored at 4 °C for 1 h prior to use in each set of antibacterial assessment experiments in this study. Serial dilution and spread plate cultivation method on solid medium was used for counting the viable cells (CFU ml<sup>-1</sup>).

### Photocatalytic experiments

Experiments were performed to investigate the decolorization and antibacterial properties of the irradiated catalysts and nano-TiO<sub>2</sub> loaded cement disks. Additionally, control experiments without irradiation were done to determine the net effect of irradiation. In all photocatalytic experiments, a 160 W high-pressure mercury vapor lamp, emitting radiations over a wavelength range of 320–420 nm, was used as an illumination source from the top.

**Table 2** Experimental design of cement samples

Sample no.	Compositions (wt%)	
	TiO <sub>2</sub>	Super-plasticizer
1	1	0
2	5	0
3	10	0
4	1	1
5	5	1
6	10	1

## Decolorization experiments

In all photocatalytic decolorization experiments, 50 ml of dye solution with an initial pH of 6 was added to a Pyrex cylindrical batch reactor with a diameter and height of 5 and 7 cm, respectively which was operated under continuous stirring and ambient temperature. Reactor was irradiated from top and this resulted in a temperature increase up to approximately 30 °C during irradiation. To examine the decolorizing property of TiO<sub>2</sub> powder, 100 mg of TiO<sub>2</sub> was dissolved in dye solution and the mixture was sonicated by the sonicator Q500 (500 W, 110 V, 50–60 Hz) for 5 min to disperse the catalyst. The mixture was then agitated in dark for 30 min before irradiation. Some decolorization experiments were also performed by using nano-TiO<sub>2</sub> loaded cement disks. Additionally, three control experiments: TiO<sub>2</sub> powder in dark, without TiO<sub>2</sub> in light and cement disk without TiO<sub>2</sub> in light were performed for comparison purposes. To investigate the effect of super-plasticizer, a final experiment was done with nano-TiO<sub>2</sub> loaded cement disks supplemented with polycarboxylic copolymer. All experiments were performed in triplicate. The dye concentration was checked by using a UV–VIS spectrophotometer (SHIMADZU, UV-2700).

## Disinfection experiment

Experiments were designed to investigate the effect of TiO<sub>2</sub> and super-plasticizer in cement disks as well as irradiation on antibacterial activity as listed in Table 3.

All materials used in these experiments were autoclaved at 121 °C for 20 min to ensure sterility. The photocatalytic experimental setup as seen in Fig. 1, consisted of a shaker, a UV lamp and an air-cooling fan to reduce the temperature developed during irradiation.

This set up was placed in a laminar air flow hood to maintain sterile environment. In this set of experiments, several 100 ml bottles each containing 20 ml bacterial suspension ( $N_0 = 10^8$  CFU ml<sup>-1</sup>) and 5 identical cement disks were placed on the shaker at 50 rpm. Samples were taken at specified times and analyzed to examine

**Table 3** Design of disinfection experiments with cement disks

Sample no.	Variable		
	Irradiation	TiO <sub>2</sub> (%)	Super-plasticizer (%)
1	+	1	0
2	+	5	0
3	+	10	0
4	–	0	0
5	–	10	0
6	+	1	1
7	+	5	1
8	+	10	1

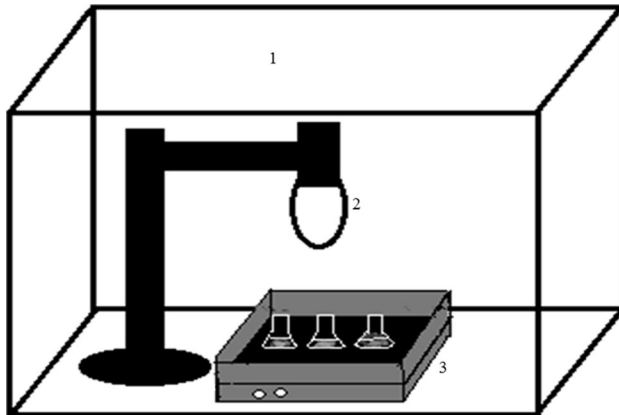


**Fig. 1** Schematic of set up used in disinfection experiments. 1 Laminar air flow hood; 2 UV light; 3 Shaking unit

the efficiency of the photocatalytic bacterial inactivation. All experiments were done in triplicate.

### Counting techniques and data presentation

To obtain the numbers of viable *E. coli* cells, a sample was taken at the end of each experiment. A series of 10-fold dilutions was then performed within 15 min and 0.1 ml of each dilution was spread on nutrient agar plate which was then incubated at 37 °C for 24 h. The observed colonies on these plates were finally counted and the colony forming units per milliliter in the original samples were calculated [27].

## Results and discussion

### XRD analysis

The XRD pattern of the synthesized TiO<sub>2</sub> catalyst is shown in Fig. 2.

It can be obviously seen that diffraction peaks appeared in the pattern are associated with a 100 % anatase phase with a proper crystalline nature. A very strong anatase peak is observed at  $2\theta$  of 25.25°, assigned to (101) plane. Other anatase peaks are observed at  $2\theta$  of 37.7° (004), 47.7° (200), 53.5° (105), 55.1° (211), 63.2° (204), 69.8° (116), 71.2° (220), and 76.1° (215) [28–30]. Among the three crystalline phases of TiO<sub>2</sub>, anatase yields the highest photocatalytic activity due mainly to its larger surface area, higher porosity and easier formation of free radicals on its particles [13, 31, 32]. The mean particle size was found to be 66.5 nm using the Debye–Scherrer equation.

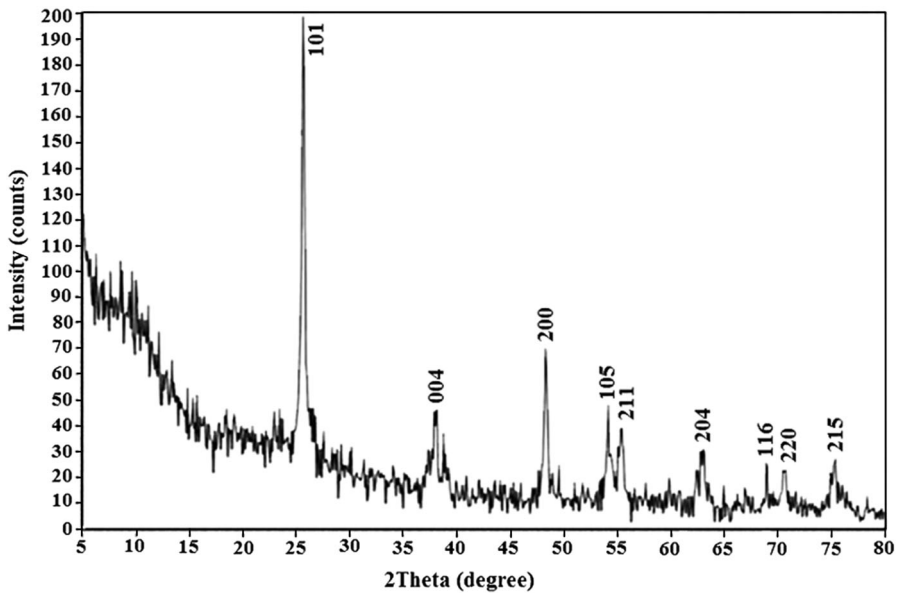


Fig. 2 XRD pattern of the synthesized nano-TiO<sub>2</sub> catalyst

### UV–Visible spectrometer analysis

UV–Vis absorption–reflection spectrum of calcined TiO<sub>2</sub> catalyst is shown in Fig. 3a.

It can be seen that the absorption spectrum of the synthesized TiO<sub>2</sub> is 395 nm which is located within the UV region. To calculate the energy gap ( $E_g$ ) for the present sample, Eq. (1) that gives the absorption coefficient of an indirect semiconductor near the absorption threshold was applied.

$$\alpha = \frac{B_i(h\nu - E_g)^m}{h\nu} \quad (1)$$

in which  $\alpha$ ,  $E_g$ ,  $h$ ,  $B_i$ , and  $\nu$  are the absorption coefficient, energy gap, the Planck's constant, the absorption constant, and the frequency of the light, respectively. Also  $m$  is an index that can be 1/2, 3/2, 2, and 3. Normally  $m$  for nanomaterials is 2. According to data from 320 to 790 nm presented in Fig. 3a,  $(\alpha h\nu)^{0.5}$  curve was plotted versus photon energy in Fig. 3b. The value of  $E_g$  has been estimated by taking the intercept of the extrapolation to zero absorption with photon energy axis [31]. In this way,  $E_g$  was obtained 2.85 eV. However, the normal energy gap is about 3.2 eV. A possible explanation for this change in energy gap can be related to the particle size. Based on Lin et al. [33], the bulk defects induced localization of molecular orbitals in the conduction band edge and create shallow/deep traps in electronic energy, in turn causing the shift of the absorption spectra. When crystalline size increases, the traps shifted to lower energy, which resulted in shifting of the absorption spectra. Also, Choudhury and Choudhury [34] have assigned the



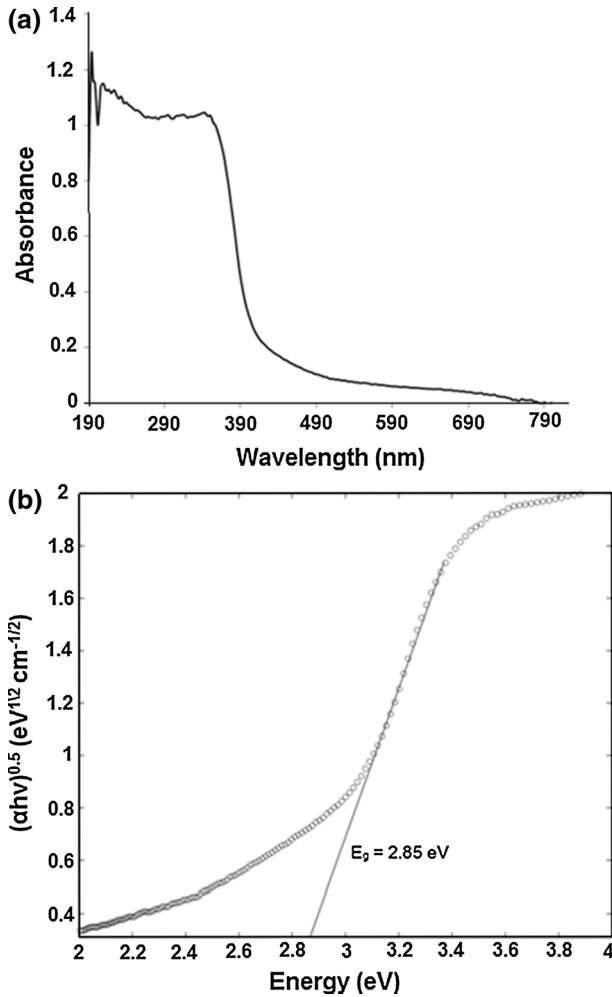


**Fig. 3** **a** UV-Vis absorption–reflection spectrum of calcined TiO<sub>2</sub> catalyst, **b** curve of  $(\alpha h\nu)^{0.5}$  versus photon energy for the estimation of energy gap of the sample

shifts to absorption wave length and reported various energy gaps in the range of 2.2–2.8 eV.

### Microstructural characterization

The field emission scanning electron microscopy images of the synthesized calcined TiO<sub>2</sub> nanoparticles are shown in Fig. 4. As it is seen, the morphology of the TiO<sub>2</sub> nanoparticles is mainly spherical with a relatively good distribution and uniformity. The mean particle size was estimated at an approximate value of 59 nm by employing the multi-crystalline software.

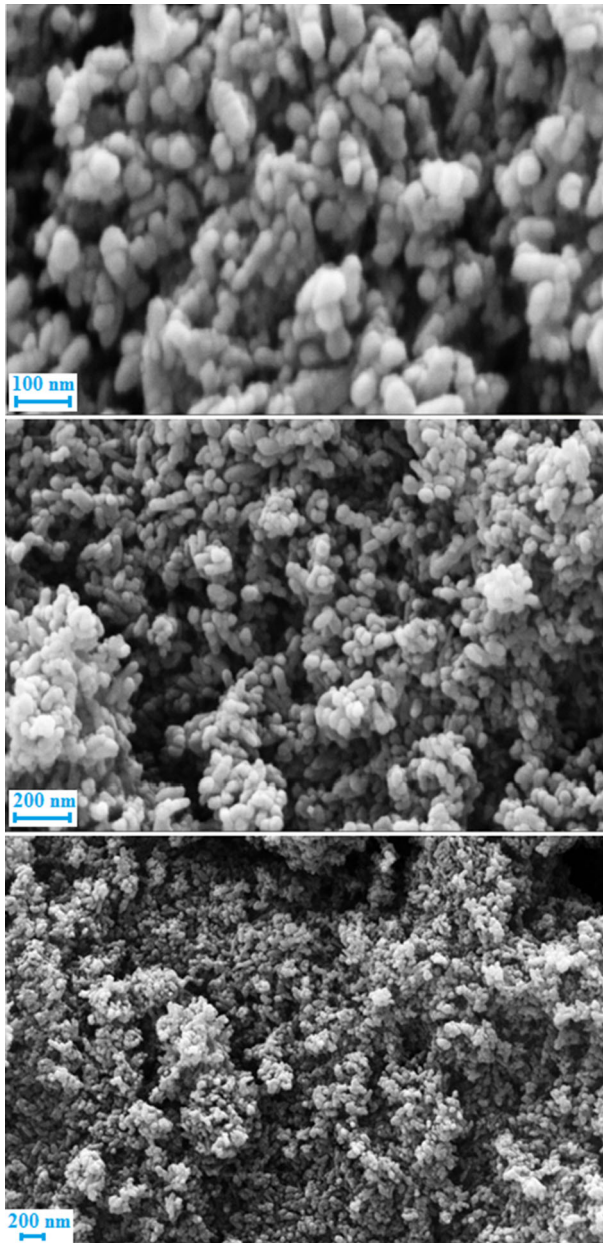


**Fig. 4** FE-SEM images of calcined TiO<sub>2</sub> catalyst

Transmission electron microscopy (TEM) image of nano-TiO<sub>2</sub> is shown in Fig. 5. From this figure, it can also be observed that the morphology of these nanoparticles is relatively spherical. The TEM analysis revealed that the nanoparticles have been formed with the size of a bit larger than 50 nm.

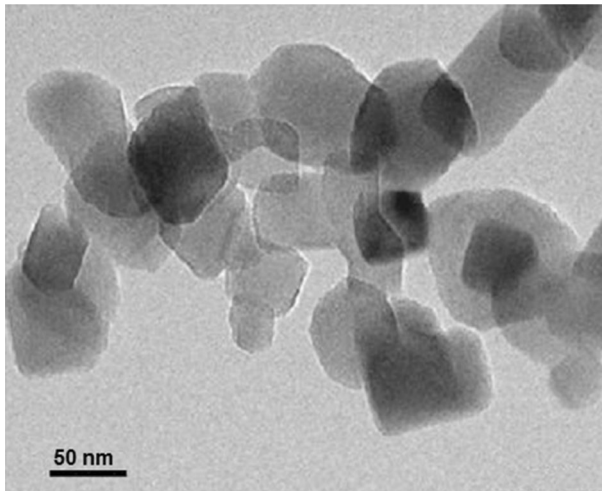


**Fig. 5** TEM image of synthesized TiO<sub>2</sub> nanoparticles

### Surface area measurement by BET method

Table 4 lists the result of surface area measurement performed on the calcined TiO<sub>2</sub> catalyst.

### Photocatalytic dye decolorization by catalyst-loaded cement disks

Time courses of dye decolorization in the presence of cement samples containing 1, 5 and 10 wt% TiO<sub>2</sub> catalyst are compared in Fig. 6a.

All nano-TiO<sub>2</sub> loaded samples showed increased initial decomposition rates compared to the control sample without TiO<sub>2</sub>. Significant enhancements were observed in the overall decolorization efficacies by increasing the amount of catalyst up to 5 %, most possibly due to the increased surface area available to the dye molecules. However, further increase in the amount of catalyst to 10 wt% barely affected the dye removal efficiency. Therefore, one can conclude that 5 % catalyst leading to 98 % color removal during 60 min is the most appropriate amount of catalyst based on the economical consideration. Photocatalytic decolorization efficiency of nano-TiO<sub>2</sub> loaded cement samples are shown in Table 5.

**Table 4** TiO<sub>2</sub> specific surface area measurement by BET method

Temperature (°C)	Porosity volume (cm <sup>3</sup> g <sup>-1</sup> )	Surface area (m <sup>2</sup> g <sup>-1</sup> )
500	0.1278	64.352
450	0.1322	67.208
400	0.7711	75.643

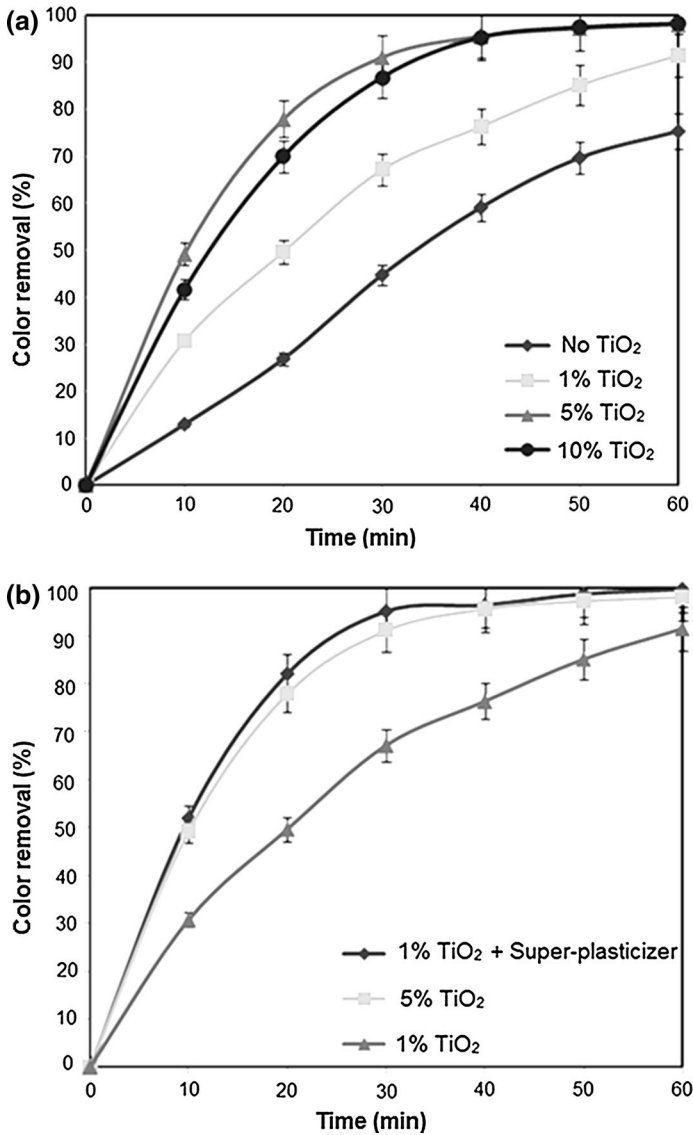


**Fig. 6** **a** Effect of TiO<sub>2</sub> in cement samples on photocatalytic dye decolorization, **b** effect of super-plasticizer on photocatalytic dye decolorization by cement samples

The effect of super-plasticizer in cement samples on dye decomposition is shown in Fig. 6b. Super-plasticizers disperse particles and contribute to further distribution of the catalyst powder within the cement mixture and prevent agglomeration which in turn improves the photocatalytic decolorization efficacy. Results show that the performance of the sample containing super-plasticizer and 1 wt% TiO<sub>2</sub> is equivalent to that of samples with no super-plasticizer and 5 wt% TiO<sub>2</sub>. Super-

**Table 5** Photocatalytic decolorization efficiency of nano-TiO<sub>2</sub> loaded cement samples

Catalyst amount (%)	Efficiency (%)
0	60.6
1	85.9
5	98.2
10	98.2

plasticizer can therefore help reducing the amount of TiO<sub>2</sub> and hence the production cost.

### Decolorization kinetics of green dye by nano-TiO<sub>2</sub> loaded cement

Generally, decomposition rate of organic compounds exposed to light under the influence of a catalyst follows the Langmuir–Hinshelwood (Eq. 2) which assumes that the reactions take place at the surface of the catalyst particles [35]. At low concentrations this equation can be simplified to a first order equation (Eq. 3).

$$r = -\frac{dC}{dt} = \frac{kKC}{1 + KC} \quad (2)$$

$$\ln\left(\frac{C}{C_0}\right) = kKt = K_{app}t \quad (3)$$

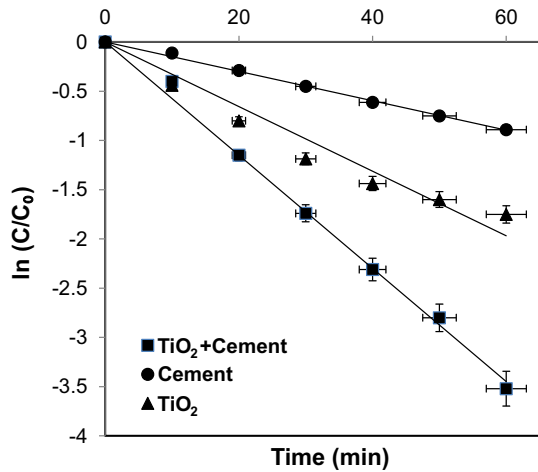
in which parameters and variables are:  $r$ , reactant oxidation rate ( $\text{mg l}^{-1} \text{min}^{-1}$ );  $C_0$ , reactant initial concentration ( $\text{mg l}^{-1}$ );  $C$ , reactant concentration at time  $t$  ( $\text{mg l}^{-1}$ );  $t$ , irradiation time (min);  $k$ , reaction rate constant ( $\text{mg min}^{-1}$ ) dependent on solute properties and reaction conditions;  $K$ , dye adsorption coefficient ( $\text{l mg}^{-1}$ ) and  $K_{app}$ , apparent rate constant ( $\text{min}^{-1}$ ) [36].

To examine the kinetics of photocatalytic decolorization of green dye by the synthesized nano-TiO<sub>2</sub> loaded cement sample,  $\ln(C/C_0)$  was plotted versus  $t$  in Fig. 7. The observed linear relationship confirms that the Malachite green dye decolorization follows a first order kinetics. According to Eq. (3), the apparent reaction rate constant is equivalent to the slope of this line which equals to  $5.7 \times 10^{-2} \text{min}^{-1}$ .

In order to identify the contribution of the catalyst in the cement sample containing this catalyst on decolorization, the results of two control experiments one with catalyst-free cement and the other with catalyst powder are also shown in Fig. 7. The apparent reaction rate constants are compared in Table 6.

It can be seen that catalyst-free cement has the lowest decolorization rate as expected. The catalyst-loaded cement showed a higher rate constant as compared to catalyst powder. This can be attributed to the presence of some elements such as iron in the cement samples and their effects on decolorization process. Photocatalytic decomposition kinetics of some other dyes such as azo dyes at low concentration by TiO<sub>2</sub> is also shown to follow a first order equation (Eq. 3) [37, 38].

**Fig. 7** Kinetics of photocatalytic decolorization of dye by catalyst powder and catalyst-loaded cement samples



### Photocatalytic inactivation of *E. coli* by catalyst-loaded cement

Photocatalytic inactivation of *E. coli* by cement samples containing 1, 5 and 10 wt% TiO<sub>2</sub> was investigated under UV irradiation. Four different control experiments were also carried out to identify the individual effect of various factors affecting bacterial inactivation. Two control experiments were done to examine the natural inactivation and bacterial inactivation under UV alone. Two other controls were used to see the effect of cement alone and catalyst (10 wt%)-loaded cement in dark. All cement samples were exposed to water flow for at least one month to reduce the pH from 12 to 7 prior to bacterial inactivation experiments to prevent alkaline pH which could in turn affect the viability of bacteria. Results of these experiments are compared in Fig. 8.

It can be seen that during the short period of these experiments (45 min), very low natural bacterial inactivation was observed. Additionally, little inactivation was detected when cement alone and catalyst-loaded cement samples were applied in the dark. Therefore, it can be concluded that TiO<sub>2</sub> barely acts as a photocatalyst in dark. Moreover, it was observed that UV irradiation alone only slightly affects bacterial inactivation. However, cement samples containing catalyst at various amounts led to a considerable bacterial inactivation under UV irradiation. Although increasing the amount of catalyst in cement samples resulted in an enhanced inactivity of bacterial

**Table 6** Comparison of the calculated apparent reaction rate constants for dye decolorization

Catalyst	$K_{app} (\times 10^{-2} \text{ min}^{-1})$	$R^2$
TiO <sub>2</sub> -loaded cement	5.7	0.997
TiO <sub>2</sub> powder	3.0	0.986
TiO <sub>2</sub> -free cement	1.0	0.944

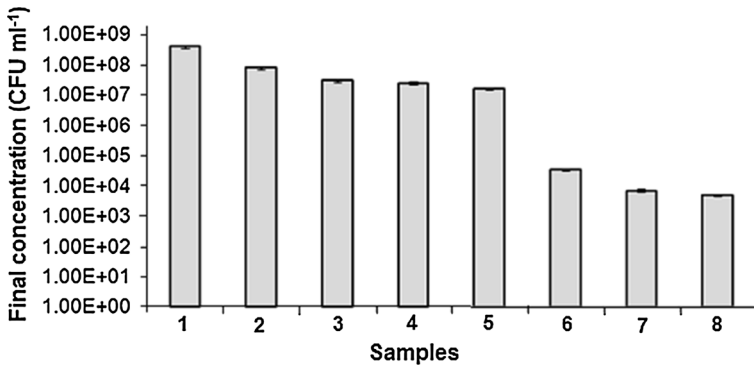


**Fig. 8** Photocatalytic inactivation of *E. coli* by cement samples containing various amounts of TiO<sub>2</sub>: 1 initial concentration, 2 *E. coli*, 3 cement/dark, 4 10 %TiO<sub>2</sub> + cement/dark, 5 UV alone, 6 1 %TiO<sub>2</sub> + UV + cement, 7 5 %TiO<sub>2</sub> + UV + cement, and 8 10 %TiO<sub>2</sub> + UV + cement

species, this effect was considerable up to 5 wt% TiO<sub>2</sub> and further increase to 10 wt% had only insignificant effect. Thus, 5 wt% TiO<sub>2</sub> can be selected as the most appropriate amount of catalyst in the cement samples for inactivation of *E. coli*. The effect of addition of 1 wt% super-plasticizer to nano-TiO<sub>2</sub> loaded cement samples containing 1, 5 and 10 wt% TiO<sub>2</sub> on bacterial inactivation under UV irradiation was also investigated. Results in Fig. 9a show that super-plasticizer positively affects bacterial inactivation, particularly at 10 wt% TiO<sub>2</sub> where the highest difference can be observed.

This can be explained by the fact that super-plasticizer can enhance catalyst dispersion in samples by preventing agglomeration of catalyst in cement pastes. This in turn improves the chance of contact between photocatalyst and bacteria. As can be seen in Fig. 9a, the performance of sample containing 5 wt% TiO<sub>2</sub> and super-plasticizer is better than that of sample with 10 wt% catalyst and without super-plasticizer. Hence, application of super-plasticizer in photocatalytic cement is strongly suggested.

The effect of the initial *E. coli* concentration on bacterial inactivation by cement samples under UV irradiation at three initial cell concentrations is shown in Fig. 9b. It can be seen that by raising the initial cell concentrations, complete inactivation occurs at longer period of time. Over the 45 min of these experiments, the overall rates of inactivation were evaluated as  $8.9 \times 10^7$ ,  $1.3 \times 10^5$  and  $1.8 \times 10^3$  CFU min<sup>-1</sup> ml<sup>-1</sup> at initial cell concentrations of  $4.00 \times 10^8$ ,  $6.00 \times 10^6$  and  $8.20 \times 10^4$  CFU ml<sup>-1</sup>, respectively. This shows the direct effect of cell concentration on the rate of the photocatalytic cell inactivation. Therefore, a rate expression of order  $n$  is assumed for cell inactivation [39] as given in Eq. (4):

$$R = k'c^n \quad (4)$$

where  $R$ ,  $k'$ ,  $c$  and  $n$  are the rate of cell inactivation, rate constant, cell concentration, and reaction order, respectively. Parameters  $n$  and  $k'$  can then be estimated

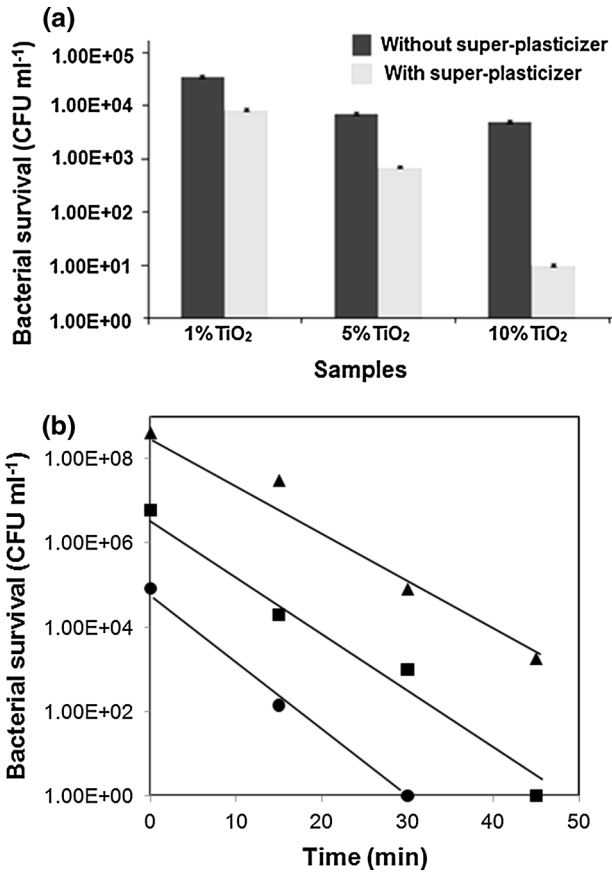


**Fig. 9** **a** Comparison of bacterial survival by nano-TiO<sub>2</sub> loaded cement samples without and with 1 wt% super-plasticizer under UV irradiation, **b** effect of the initial *E. coli* concentration on time course of inactivation by TiO<sub>2</sub>

according to Eq. (5) by plotting  $\log(R)$  versus  $\log(c)$  in Fig. 10 and finding the slope and intercept of the line, respectively.

$$\log(R) = \log(k') + n \log(c) \quad (5)$$

This plotting resulted in a line with a slope of 0.995 and intercept of  $-0.87$ .

This reveals that the photocatalytic bacterial inactivation by nano-TiO<sub>2</sub> loaded cement well follows a first order rate expression with a rate constant of  $0.135 \text{ min}^{-1}$ . Some recent studies have shown that at high cell concentrations ( $>10^7 \text{ CFU ml}^{-1}$ ), a fraction of cells could escape from UV exposure due to both shielding of microorganisms and a poor mixing [40]. The tailing observed in certain inactivation curves has also been attributed to the presence of a small sub-population of the organism which are more resistant to the effects of UV radiation, than the bulk population due to their genetic or morphological properties [40].



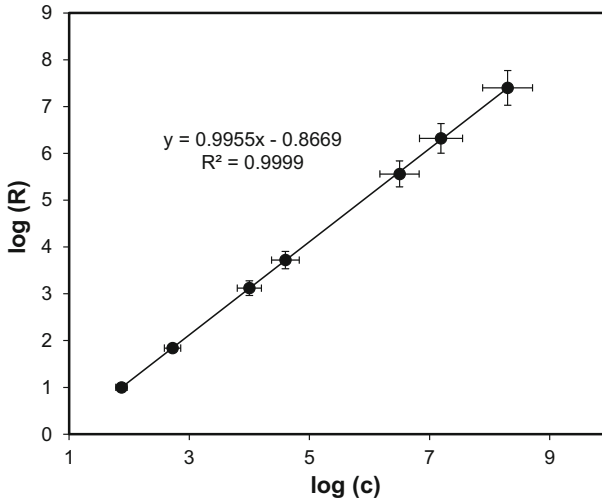


**Fig. 10** Overall rates of inactivation versus bacteria concentration

## Conclusions

Experimental results showed that cement samples containing TiO<sub>2</sub> nanoparticles exhibit stronger photocatalytic properties compared to the same amount of pure TiO<sub>2</sub> nanoparticles under UV irradiation. Taking into account that only a small amount of the TiO<sub>2</sub> powder mixed with cement paste lies on sample surface and only this part contributes to the photocatalytic activities, one can conclude that the required amount of TiO<sub>2</sub> in cement is much less than the amount of pure powder. Although improvements were observed in photocatalytic properties by raising the catalyst in the cement samples, addition of 5 wt% catalyst to cement paste is recommended based on the cost and performance efficiencies. Moreover, it was shown that addition of a super-plasticizer could enhance the organic pigment decolorization and microorganism inactivation due to the improved dispersion of catalyst particles and this in turn reduces the required catalyst to 1 wt% and hence makes the process more cost-effective. Therefore, nano-TiO<sub>2</sub> loaded cement can be efficiently applied as an antibacterial/decolorizing coating on the intended surfaces.

### Compliance with ethical standards

**Conflict of interest** No conflict of interest has been expressed by authors.

**Animal and human rights** The research was not involved in human or animal participants.

## References

1. T. Yuranova, V. Sarria, W. Jardim, J. Rengifo, C. Pulgarin, G. Trapesinger, J. Kiwi, J. Photochem. Photobiol. **188**, 334–341 (2007)

2. W. Zhu, P.J.M. Bartos, A. Porro, *Mater. Struct.* **37**(9), 649–658 (2004)
3. J. Chen, C.S. Poon, *Buil. Environ.* **44**, 1899–1906 (2009)
4. O. Carp, C.L. Huisman, A. Reller, *Prog. Solid State Chem.* **32**, 33–177 (2004)
5. G. Sen, W.U. ZhongBiao, Z. WeiRong, *Chin. Sci. Bull.* **54**(7), 1137–1142 (2009)
6. R. Wang, K. Hashimoto, A. Fujishima, M. Chikuni, E. Kojima, A. Kitamura, M. Shimohigoshi, T. Watanabe, *Nat.* **388**, 431–432 (1997)
7. C.S. Poon, *Constr. Build. Mater.* **21**(8), 1746–1753 (2007)
8. J.T. Sil, K.G. Man, W.S. Yong, Korea Patent 1020010100052, (2001)
9. L. Berkeley, *Pier final project report* (California Energy Commission, California, 2008)
10. H. Sun, C. Wang, S. Pang, X. Li, Y. Tao, H. Tang, M. Liu, *J. Non-Cryst. Solids* **354**, 1440–1443 (2008)
11. Proceedings of the 2nd international symposium on nanotechnology in construction (Eds: Y. de Miguel, A. Porro, P. J. M. Bartos), RILEM Publications SARL (2005)
12. Proceedings of the RILEM international symposium on environment-conscious materials and systems for sustainable development (Eds: N. Kashino, Y. Ohama), RILEM Publications SARL (2004)
13. R.L. Narayana, M. Matheswaran, A. Abd Aziz, P. Saravanan, *Desalination* **269**(1–3), 249–253 (2011)
14. W. Wang, L. Zhang, T. An, G. Li, H.Y. Yip, P.K. Wong, *Appl. Catal. B-Environ.* **108–109**, 108–116 (2011)
15. H. Kominami, H. Kumamoto, H. Kera, O. Bunsho, *J. Photochem. Photobiol., A* **160**(1–2), 99–104 (2003)
16. A.L. Clovis, J.C. Glenda, B.L. David, J.O. Anthony, K.S. Darlene, A.S. Lisa, *Environ. Sci. Technol.* **34**(22), 4754–4758 (2000)
17. A. Kubacka, M. Ferrer, A. Martinez-Arias, M. Fernandez-Garcia, *Appl. Catal. B-Environ.* **84**(1–2), 87–93 (2008)
18. H. Tao, W. Wei, S. Zhang, *J. Photochem. Photobiol., A* **161**(2–3), 193–199 (2004)
19. N. Baram, D. Starosvetsky, J. Starosvetsky, M. Epshtein, R. Armon, Y. Eineli, *Appl. Catal. B-Environ.* **101**(3–4), 212–219 (2011)
20. T. Sato, Y. Koizumi, M. Taya, *Biochem. Eng. J.* **14**(2), 149–152 (2003)
21. L. Caballero, K.A. Whitehead, N.S. Allen, J. Verran, *J. Photochem. Photobiol., A* **202**(2–3), 92–98 (2009)
22. S. Srivastava, R. Sinha, D. Roy, *Aquat. Toxicol.* **66**, 319 (2004)
23. B.H. Hameed, M.I. El-Khaiary, *J. Hazard. Mater.* **154**, 237 (2008)
24. A.S. Bojinova, C.I. Papazova, I.B. Karadjova, I. Poullos, *Eurasian. J. Anal. Chem.* **3**(1), 34–43 (2008)
25. C.C. Chen, C.S. Lu, Y.C. Chung, J.L. Jan, *J. Hazard. Mater.* **141**, 520–528 (2007)
26. R.M. Pratap, A. Venugopal, M. Subrahmanyam, *Water Res.* **41**(2), 379–386 (2007)
27. F. Malekzadeh, M. Shahamat, *General Microbiology*, 4th edn (Aghigh Press, Iran, 1997)
28. H.S. Nalwa, *Handbook of Advanced Electronic and Photonic Materials and Devices* (Academic Press, USA, 2001)
29. K.M. Reddy, S.V. Manorama, A.R. Reddy, *Mater. Chem. Phys.* **78**(1), 239–245 (2003)
30. A. Fujishima, X. Zhang, *CR. Chim.* **9**(5–6), 750–760 (2006)
31. J.M. Kwon, Y.H. Kim, B.K. Song, S.H. Yeom, B.S. Kim, J.B. Im, *J. Hazard. Mater.* **134**(1–3), 230–236 (2006)
32. J. Hagen, *Industrial Catalysis*, 2nd edn. (Wiley-Vch, Germany, 2006)
33. H. Lin, C.P. Huang, W. Li, C. Ni, S. Ismat Shah, Y.H. Tseng, *Appl. Catal. B-Environ.* **68**, 1–11 (2006)
34. B. Choudhury, A. Choudhury, *Physica E.* [10.1016/j.physe.2013.10.014](https://doi.org/10.1016/j.physe.2013.10.014)
35. J. Chanathaworn, C. Bunyakan, W. Wiyaratn, J. Chungsiriporn, Songklanakarin. *J. Sci. Technol.* **34**(2), 203–210 (2012)
36. I.K. Komstantinou, T.A. Albanis, *Appl. Catal. B-Environ.* **49**(1), 1–14 (2004)
37. N. San, A. Hatipoglu, G. Kocturk, Z. Cinar, *J. Photochem. Photobiol., A* **139**(2–3), 225–232 (2001)
38. M. Saquib, M. Muneer, *Dyes Pigments* **53**(3), 237–249 (2002)
39. A.G. Rincon, C. Pulgarin, *Appl. Catal. B-Environ.* **49**(2), 99–112 (2004)
40. S.A. Craik, D. Weldon, G.R. Finch, J.R. Boltman, M. Belosevic, *Water Res.* **35**(6), 1387–1398 (2001)